Polymer Journal

REGULAR ARTICLE

Special Issues –International Symposium on Polymer Crystallization 2007–

Kinetic Roughening Transition of *isotactic* Polybutene-1 Tetragonal Crystals: Disagreement between Morphology and Growth Kinetics

By Motoi YAMASHITA and Takuya TAKAHASHI*

The morphology and lateral growth rate of *isotactic* polybutene-1 (*it*-PB1) tetragonal crystals have been investigated for crystallization from the melt over a wide range of crystallization temperature from 50 to 110 °C. The morphology of *it*-PB1 tetragonal crystals is rounded shape at crystallization temperatures lower than 85 °C, while lamellar single crystals possess faceted morphology at higher crystallization temperatures; the kinetic roughening transition occurs around 85 °C. Regime II growth mode on faceted growth fronts does not work below 85 °C, since the growth faces are rough; the morphology is indicative of regime III growth on rough surfaces. However, the growth rate shows single temperature dependence derived from the nucleation theory; it does not present regime II-III transition. Possible mechanisms for the crystal growth of *it*-PB1 tetragonal phase are discussed.

KEY WORDS: *Isotactic* Polybutene-1 / Tetragonal Phase (form II) / Melt Crystallization / Growth Rate / Kinetic Roughening / Morphology /

For polymers as well as low-molecular-weight materials, crystallization mechanisms have been investigated through the morphology and growth rate of crystals. The thickness of the lamellar crystals is an important quantity describing the morphology specific to polymer crystals. It is well known that the thickness l decreases with supercooling ΔT,[1,2]

$$l_c = \frac{2\sigma_e}{\Delta g} + \delta l_c = \frac{2\sigma_e T_m^0}{\Delta h_f \Delta T} + \delta l_c \quad (1)$$

where Δg is the difference of free energies between crystal and liquid phases, namely, the driving force of crystallization, which is proportional to supercooling $\Delta T = T_m{}^0 - T$ ($T_m{}^0$ is the equilibrium melting temperature), σ_e is the end-surface free energy per unit area, Δh_f is the heat of fusion per unit volume of crystal and δl_c is a constant length independent of supercooling. The first term in eq 1 is the minimum thickness for the lamellar crystal to grow; the crystal with this thickness is in equilibrium with the melt in a supercooling of ΔT. Eq 1 has a clear meaning that the lamellar thickness of a growing crystal must be thicker by δl_c than the minimum thickness.

Another important feature of crystallization of polymers as well as organic or inorganic materials with low molecular weight is the supercooling dependence of the growth rate of the crystals. The growth rate G observed can be expressed as follows:

$$G = G_0 \exp\left[-\frac{U}{R(T - T_V)}\right] \exp\left[-\frac{K}{T\Delta T}\right] \quad (2)$$

where K is a constant, U is the 'activation' energy for polymer diffusion, $R = kN_A$, (k is the Boltzmann constant and N_A is Avogadro's number) T_V is the Vogel temperature ($= T_g - 30$ (K), T_g is the glass transition temperature). G_0 is a factor almost independent of ΔT, the first exponential factor is the Vogel–Fulcher factor for viscosity, and the second exponential factor is the surface kinetic factor derived originally from the nucleation theory of Lauritzen–Hoffman.[1,2]

According to the nucleation theory,[1] the barrier of surface nucleation is thought of as the work $2b\sigma l$ of building the two lateral surfaces of a surface nucleus, *i.e.*, nucleating stem (b is the layer thickness and σ is the side-surface free energy per unit area). The surface nucleation rate i is given by the following equation:

$$i \propto \exp\left[-\frac{2b\sigma l_c}{kT}\right] \cong \exp\left[-\frac{4b\sigma\sigma_e T_m^0}{k\Delta h_f T\Delta T}\right] \equiv \exp\left[-\frac{K_{nuc}}{T\Delta T}\right] \quad (3)$$

The barrier of step propagation has been interpreted as the chain folding free energy q, which is independent on temperature. Step propagation velocity $g \propto \exp[-q/kT]$ is hence assumed to be almost constant in the temperature range of observation.[1]

In the regime of multiple nucleation, regime II, on flat growth fronts (facets), the surface kinetic factor of the growth rate is given by the following equation[3]

$$G_{II} = b(2ig)^{1/2} \quad (4)$$

Since g is assumed to be almost constant in the nucleation theory,[1] K in eq 2 is represented by the following equation

$$K = \frac{K_{nuc}}{2} = \frac{2b\sigma\sigma_e T_m^0}{k\Delta h_f} \equiv K_{II} \quad (5)$$

The nucleation theory therefore successfully explains the observed supercooling dependence of growth rate expressed by eq 2.

Department of Bioscience and Bioinformatics, Ritsumeikan University, 1-1-1 Noji-higashi, Kusatsu 525-8577, Japan
*To whom correspondence should be addressed (Present address: Department of Pharmacy, Ritsumeikan University, Tel: +81-77-561-2658, Ext. 8427, Fax: +81-(0)77-561-2659, E-mail: motoi-y@fc.ritsumei.ac.jp).

With decreasing temperature, growth fronts become kinetically roughened due to increasing surface nuclei. Growth shape loses its facets and presents rounded morphology, which is called kinetic roughening transition. Growth mode changes from regime II on flat growth fronts to regime III on rough surfaces.[1] In regime III growth, the growth rate is directly proportional to the nucleation rate i; K in eq 2 is given as follows.[1]

$$K = K_{\mathrm{nuc}} = \frac{4b\sigma\sigma_{\mathrm{e}}T_{\mathrm{m}}^{0}}{k\Delta h_{\mathrm{f}}} = 2K_{\mathrm{II}} \equiv K_{\mathrm{III}} \tag{6}$$

Around the regime II-III transition, the magnitude of slope K in $\ln G + U/R(T - T_{\mathrm{v}})$ *vs.* $1/T\Delta T$ plot gradually increases and becomes a value twice as large as K_{II}. Regime II-III transition is reported in polyethylene (PE),[4] *isotactic* polypropylene (*it*-PP),[5] and poly(*L*-lactic acid) (PLLA).[6]

In 1992, a paradox was reported on the crystallization of *isotactic* polystyrene (*it*-PS) in solutions and in the melt by Tanzawa *et al.*[7,8] In *it*-PS crystal growth, regime II-III transition is not observed while kinetic roughening transition is clearly observed; growth rate presents the same temperature dependence described by eq 2 both for faceted and rounded crystals. We have investigated the crystallization of *isotactic* polybutene-1 (*it*-PB1) in the melt.[9–16] *It*-PB1 exhibits stable trigonal form (I) with 3/1 helical chains and metastable tetragonal form (II) with 11/3 helical chains as the most common structures.[17,18] Crystallization in the bulk melt under atmospheric pressure yields the tetragonal form.[17] When stored at room temperature, the tetragonal phase undergoes a solid-solid transformation into the trigonal phase.[18] In this paper, we focus on the crystallization of the tetragonal crystals, and report the growth rate and morphology of *it*-PB1 tetragonal crystals grown in the melt. We observed that kinetic roughening transition does not accompany regime II-III transition for *it*-PB1 tetragonal phase, either. We will discuss the possible mechanisms for the crystal growth of the *it*-PB1 tetragonal phase.

EXPERIMENTAL

The *it*-PB1 used in this study was purchased from Scientific Polymer Product ($M_{\mathrm{n}} = 47450$, $M_{\mathrm{w}} = 181700$; $M_{\mathrm{w}}/M_{\mathrm{n}} = 3.83$; melt index is 20 g/10 min). *In situ* observations of the crystallization process were carried out using an optical microscope (Nikon OPTIPHOT2) with a hot-stage (Mettler FP82). Films of *it*-PB1, *ca.* 50 μm thick, between two cover glasses were melted at 140 °C for 2 min and cooled to a crystallization temperature between 50 °C and 110 °C. The growth rate was determined from the time dependence of the radius of spherulites or the major axis of axialites.

Small angle X-ray scattering (SAXS) photographs were taken with a SAXS camera (camera length 414 mm) in vacuum to obtain lamellar long spacings, using an imaging plate system (Rigaku R-AXIS DSII). X-Ray used was nickel-filtered CuK_{α} radiation generated at 50 kV and 140 mA. After the subtraction of the background intensity, isotropic two-dimensional data were circularly averaged to obtain one-dimensional data, and corrected for the Lorentz factor. Films of *it*-PB1, about 500 μm in thickness, between aluminum foil were melted at 150 °C for 3 min in an oven, transferred quickly to the hot-stage kept at a crystallization temperature. The films crystallized were left at room temperature for 10 d and used for SAXS measurements. In 10 d at room temperature the spontaneous form II to I phase transition occurs without changing the lamellar thickness of the crystals. Since the crystal density of form I is larger than that of form II, SAXS intensity is much enhanced after 10 d.

Wide-angle X-ray scattering (WAXS) was performed to identify crystal structures. Nickel-filtered Cu K_{α} radiation was used, generated at 35 kV and 40 mA. The system and procedure used for data acquisition and analysis were the same as those used for SAXS experiments.

For the experiments of morphology observation, thin *it*-PB1 films were prepared by casting a *p*-xylene solution (0.1 wt % *it*-PB1) onto a carbon-coated mica. The films dried were heated up to 140 °C, cooled to a crystallization temperature and crystallized in the hot-stage for a suitable time, and quenched to room temperature. The *it*-PB1–carbon films were floated on a water surface and picked up on electron microscope grids. The *it*-PB1 crystals on the carbon film were observed by transmission electron microscopy (TEM; JEOL Ltd. JEM-1200EX II) and optical microscopy (OM) to investigate the morphology of crystals.

RESULTS AND DISCUSSION

We confirmed by WAXS measurements that samples immediately after the crystallization are in the tetragonal phase. Hence, the observed growth rate, long spacings and crystal morphology are those of crystals in the tetragonal phase. Samples stored at room temperature for 10 d after crystallization exhibited peaks characteristic of the trigonal phase.

Figure 1 shows the first-order long spacings L_1 and second-order long spacings L_2 as the functions of the inverse supercooling, $1/\Delta T$. The $1/\Delta T$ dependences of L_1 and L_2 demonstrate linearity over the whole temperature range investigated; eq 1 holds for L_1 from 40 to 100 °C and for and L_2 from 45 to 100 °C. Fu *et al.* showed that the crystallinity ϕ of *it*-PB1 takes an almost constant value of about 0.5 to 0.6 for a wide range of crystallization temperature[20] and for different molecular weights. The long spacings L_1 is the sum of crystalline layer thickness l_{c} and inter-crystalline amorphous layer thickness l_{a}. The lamellar crystal thickness l_{c} can be estimated using the equation: $l_{\mathrm{c}} = \phi L_1$. Since L_1 has linear dependence on $1/\Delta T$, l_{c} is also estimated to have a linear dependence on $1/\Delta T$ in accordance with eq 1, assuming that crystallinity ϕ is constant. The l_{c} values estimated assuming $\phi = 0.55$ are plotted in Figure 1.

Typical optical micrographs of *it*-PB1 crystals grown from the melt are shown in Figure 2. At crystallization temperatures higher than 90 °C, tetragonal, octagonal, oval and circular crystals were usually observed; they are axialites, some of

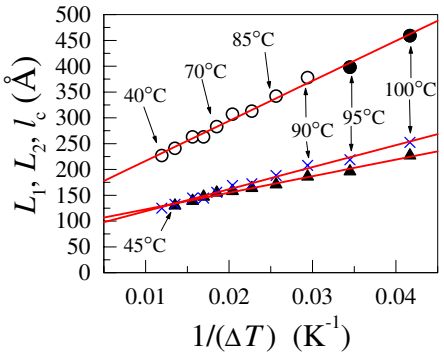

Figure 1. First-order long spacings L_1 (○), second-order long spacings L_2 (▲) and estimated values of crystal thickness l_c (×) plotted against reciprocal supercooling $1/\Delta T$. The ratios of the first-order long spacings to the second-order long spacings are about two. For samples crystallized at 90 °C, this ratio is 2.03. At 95 and 100 °C, only the second-order reflections were capable of being observed. By multiplying the second-order long spacings by the ratio at 90 °C, 2.03, we calculated the first-order long spacings at 95 and 100 °C. They are represented by filled circles (●). T_m^0 = 124 °C[19] is used to calculate ΔT.

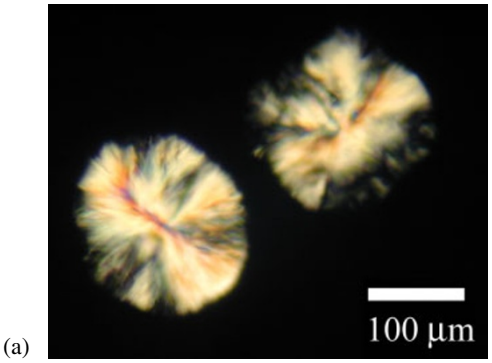

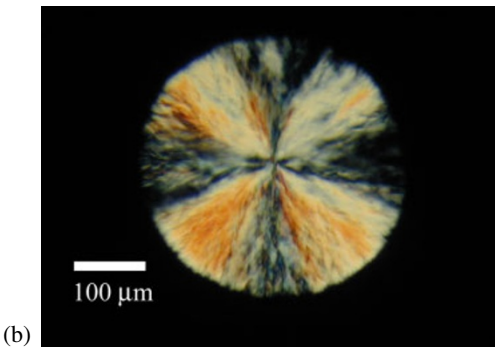

Figure 2. Optical micrographs of *it*-PB1 crystallized in the melt at 100 °C; crossed polars. (a) 140 min and (b) 180 min after the temperature reached 100 °C.

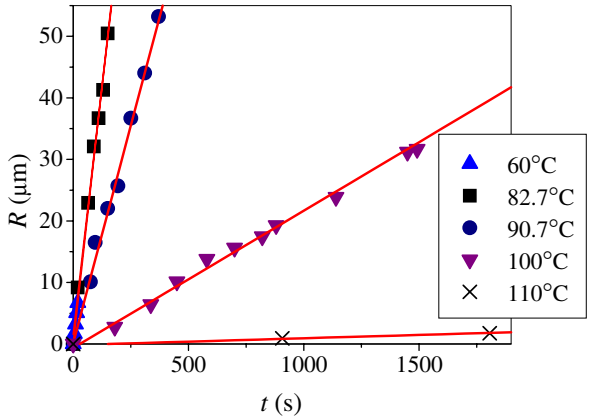

Figure 3. Time dependence of radius R for several crystallization temperatures. (▲) 60 °C, (■) 82.7 °C, (●) 90.7 °C (▼) 100 °C, (×) 110 °C.

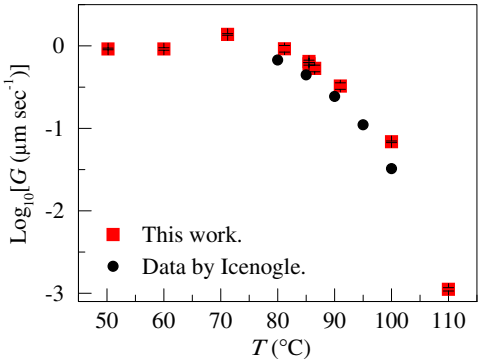

Figure 4. Growth rate G versus crystallization temperature T: (■) this work and (●) data by Icenogle.[21]

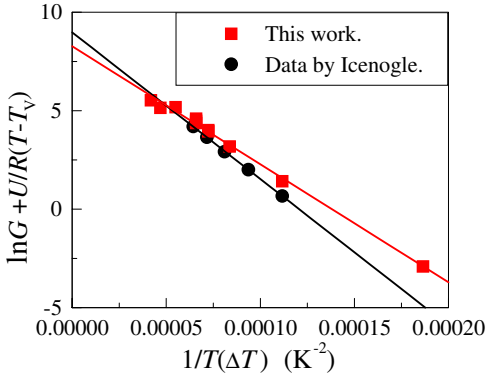

Figure 5. Plot of $\ln G + U/R(T - T_V)$ versus $1/T\Delta T$. Symbols are the same as in Figure 4. The parameters used for the plots are as follows: T_m^0 = 124 °C,[19] T_v = −84.2 °C, U/R = 758.[2]

which grew to be circular crystals. At lower crystallization temperatures, spherulites were always observed. The size of the crystals $2R$, *i.e.*, the diameter of spherulites or the major axis of axialites, was measured as a function of time t.

The radius of the spherulites or the axialites R increased linearly with crystallization time t for all the crystallization temperatures as shown in Figure 3. The growth rate G was determined from the slope of the time-radius curve. The logarithm of G is plotted against crystallization temperature in Figure 4. The results by Icenogle[21] are included for the sake of comparison. The $\log G - T$ curve is a half of the typical dome shape.

Figure 5 shows $\{\ln G + U/R(T - T_v)\}$ as a function of $1/T\Delta T$. $\{\ln G + U/R(T - T_v)\}$ depends on $1/T\Delta T$ linearly over the whole range examined; eq 2 holds for all the

crystallization temperature range investigated from 50 to 110 °C.

According to eq 2, the extrapolation to zero of the straight line in Figure 5 for $1/T\Delta T$ gives the value of $G_0 = (3.92 \pm 0.56) \times 10^3\ \mu m\ s^{-1}$; from the slope the value of K is obtained to be $(6.00 \pm 0.15) \times 10^4\ K^2$. The values of G_0 and K obtained from the data by Icenogle are $(7.94 \pm 0.30) \times 10^3\ \mu m\ s^{-1}$ and $(7.45 \pm 0.05) \times 10^4\ K^2$, respectively. The value of K is roughly in agreement with the present result. Although the G_0 value is twice larger than the present result, the G_0 values are considered to be in the same order of magnitude since the two linear dependences in Figure 5 almost overlaps each other. This can be explained on the basis of the molecular weight distribution ($M_n = 73000$, $M_w = 750000$; $M_w/M_n = 10.3$). The G_0 value has the physical meaning of growth rate when nucleation barrier is dismissed, and depends on the molecular weight distribution of the samples.[1,2] The G_0 value is smaller for larger molecular weight. Increasing the molecular weight causes increased friction between the reptating molecules and the surrounding molecules. This means that increased retardation of molecular transport onto the growth front leads to a decreasing G_0 value. On the other hand, the existence of shorter chains contained in samples with broader molecular weight distribution makes the G_0 value larger, since shorter chains decrease chain entanglements and enhances molecular transport. The M_n and M_w values used in the work by Icenogle are larger than the M_n and M_w values used in this work, respectively. The dispersion index $M_w/M_n = 10.3$ of the sample used in the work by Icenogle is much larger than that in this work, $M_w/M_n = 3.83$. This indicates that the sample used in the work by Icenogle has a much broader molecular weight distribution and contains a large fraction of shorter chains. (The M_w/M_n value approaches unity for samples with a narrow molecular weight distribution.) The larger M_n and M_w values in Icenogle's work contribute to molecular transport retardation. This is, however, cancelled by the effect of the large fraction of short chains. As the result, the G_0 values are considered to be in the same order of magnitude.

Figure 6 shows the electron micrograph and diffraction pattern of a single crystal grown at 100 °C; optical micrograph of a single crystal grown at 100 °C is also shown. There appears a square-shaped crystal with serrated edges in the electron micrograph (Figure 6a). The net pattern with four-fold symmetry in Figure 6b shows the crystal in Figure 6a is a flat-on tetragonal single crystal. Thin straight boundary lines observed inside the serrated edges show the change in lamellar thickness caused by quenching, and thereby correspond to the growth fronts of the single crystal just before quenching. The trace of well facetted {100} growth front is observed clearly in Figure 6a; faceted crystal outline appears also clearly in the optical micrograph (Figure 6c). Also observed are the sector boundaries in the {110} direction. The traces of growth fronts in Figure 6a and faceted crystal outline in Figure 6c indicate that the tetragonal single crystals are well faceted at 100 °C, and hence the tetragonal crystals grow by nucleation-controlled growth on {100} plane at 100 °C. Similar faceted morphology

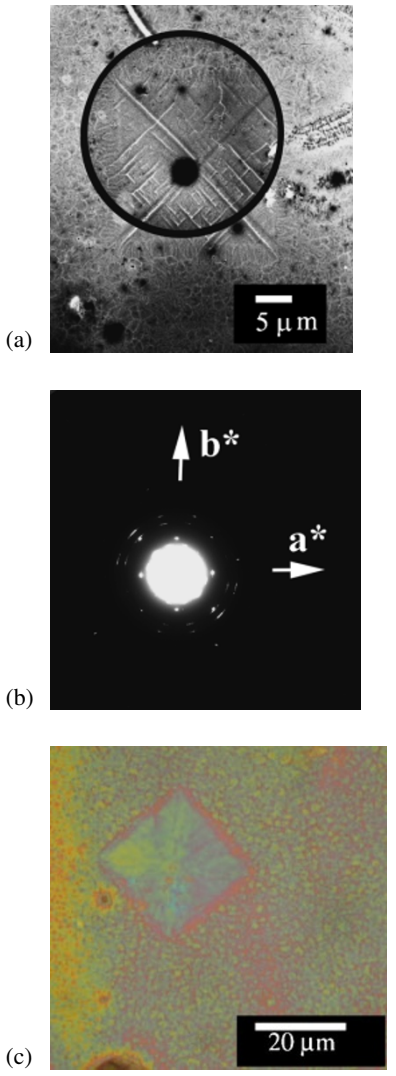

Figure 6. (a) Electron micrograph and (b) diffraction pattern of *it*-PB1 single crystal grown at 100 °C. (Taken from ref 9.) The circle in (a) shows the selected area for the diffraction. (c) Optical micrograph of *it*-PB1 single crystals grown at 100 °C.

is observed in crystals grown at 110 °C in the melt (figures not shown).

A single crystal grown at 88 °C also shows the same single-crystal net pattern as at 100 °C (Figure 7c). The trace of the growth front of the single crystal, however, slightly rounds at the sides, while the corners still remain with four-fold symmetry (Figure 7a, 7b). Sector boundaries in the {110} directions are observed.

At a further lower temperature of 85 °C, facetted morphology disappears. The growth fronts show rounded or wavy habits, indicating the growth fronts are kinetically roughened while the {110} sector boundaries are still observed (Figure 8).

Therefore, *it*-PB1 tetragonal crystals have the kinetic roughening transition temperature around 85 °C; the growth mode changes from regime II growth on facetted growth front to regime III growth on rough surface at crystallization

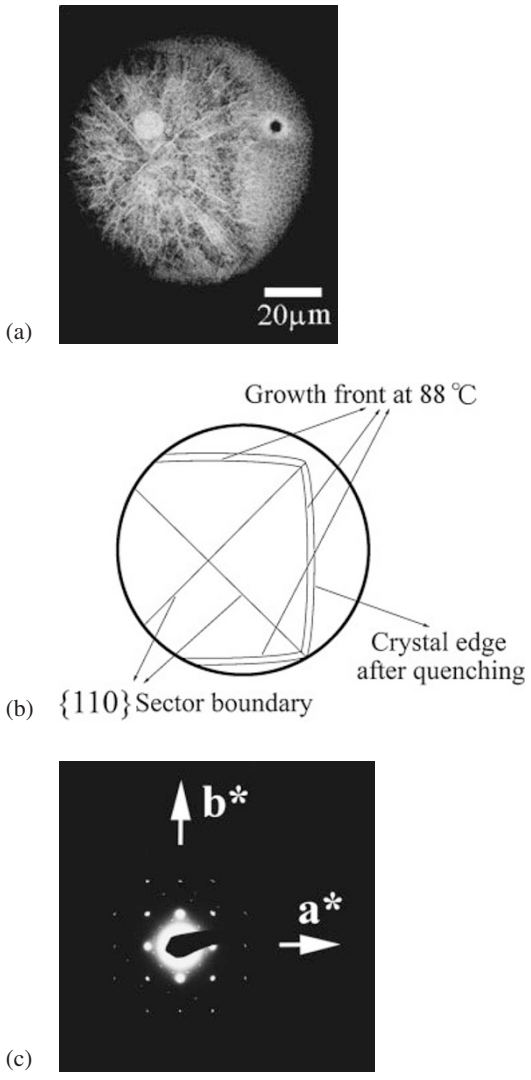

Figure 7. (a) Electron micrograph, (b) schematic illustration, and (c) diffraction pattern of *it*-PB1 single crystal grown at 88 °C. (Taken from ref 9.)

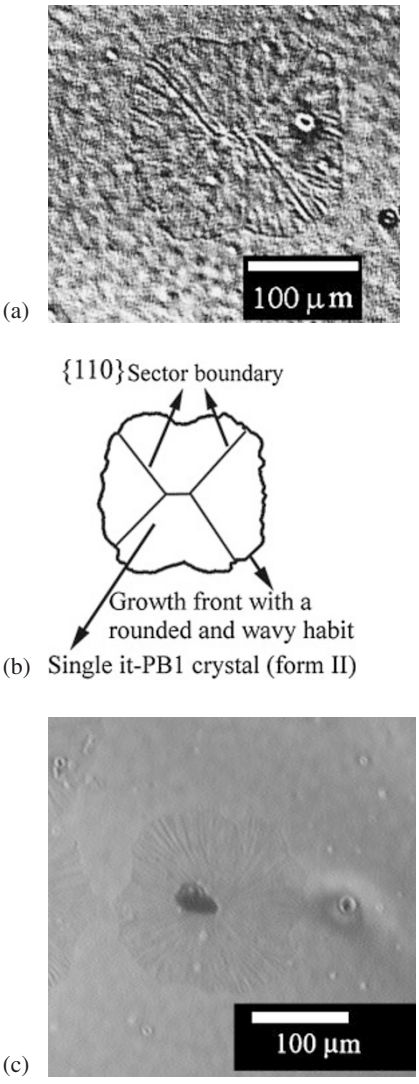

Figure 8. (a) *In situ* optical micrograph and (b) schematic illustration of an *it*-PB1 single crystal growing at 85 °C. (Taken from ref 9.) (c) Another single crystal taken at 85 °C (*in situ*; optical micrograph).

temperatures lower than 85 °C since the growth face becomes rough. This is, however, in contradiction with the single linear dependence of $\{\ln G + U/R(T - T_v)\}$ on $1/T\Delta T$ observed in Figure 5: the $1/T\Delta T$ dependence of $\{\ln G + U/R(T - T_v)\}$ does not show any transition. This is the same disagreement between the growth rate and morphological change reported by Tanzawa *et al.* in the crystal growth of *it*-PS.[7,8]

Tanzawa *et al.*[8] proposed an intermediate growth mode between nucleation controlled growth and rough surface growth to explain the absence of the regime II-III transition. They introduced 'multi-height steps' on the basis of the six-fold symmetry of *it*-PS crystal phase. The multi-height steps divide the growth face into microscopically flat but small parts as well as they work as growth faces with different growth directions. This causes the outline of the lamellar crystal to lose its anisotropy, the edge of lamellar crystals being ragged; the crystal growth shape can lose its facets continuously with the growth kinetics still keeping the temperature dependence derived from the nucleation theory. The concept of the multi-height steps and intermediate growth mode has been such a powerful solution that it successfully explained the mechanisms for dendritic growth into snowflake-shaped crystals or dense-branched morphology of *it*-PS crystals in ultrathin films[22] reported by Taguchi *et al.* The intermediate growth mode, however, can not be applied to the *it*-PB1 tetragonal phase because the tetragonal phase does not possess six-fold symmetry required for the multi-height steps.

In our previous work,[9] we performed analyses based on pinning barrier.[23,24] We reported that if crystallization of the tetragonal phase proceeds monomer by monomer, the pinning barrier can make the regime II-III transition invisible, but this seems doubtful. The tetragonal crystal phase possesses loose $11/3$ helical chains, and needs at least $11/3$ helical monomers to form one turn of helix. It is unrealistic to consider that crystallization of the tetragonal phase proceeds monomer by monomer.

The paradox of missing regime II-III transition can be solved by introducing a barrier proportional to crystal thickness l into step propagation processes. With this barrier, step propagation velocity g can have the same form of $1/T\Delta T$ dependence as nucleation rate i as follows.

$$g \propto \exp\left[-\frac{Bl}{kT}\right] \cong \exp\left[-\frac{2\sigma_e BT_m^0}{k\Delta h_f T\Delta T}\right] \equiv \exp\left[-\frac{K_{step}}{T\Delta T}\right] \quad (7)$$

where B is a constant. The expression of K_{II} in eq 5 is modified as $K_{II} = (K_{nuc} + K_{step})/2$ from eqs 3 and 4. If the K_{step} value is large enough and takes a value close to K_{nuc}, the gap between K_{II} and K_{III} decreases, which can eventually make the regime II-III transition invisible.

The barrier proposed above is a generalization of 'segmentalized-aligned' activated state originally proposed by Hoffman and Miller[1] to explain the nucleation barrier proportional to l. They assumed that a polymer chain needs to pass through a 'segmentalized and aligned' activated state, *i.e.*, needs to be elongated along the growth face without actual crystallographic attachment before they become incorporated into the crystal phase and form a surface nucleating stem. The elongation process generates a barrier proportional to l due to the loss of conformational entropy without free energy gain of crystallographic attachment. We can naturally introduce a similar 'segmentalized-aligned' activated state along steps before polymer chains become incorporated into the steps after chain folding. The 'segmentalized-aligned' chains along the steps have an entropic barrier proportional to l due to chain elongation. The elongated chains are also hypothesized to have free energy gain proportional to l due to chain-step interaction. The remainder of the entropic barrier partially cancelled by the free energy gain will serve as the barrier of step propagation proportional to l.

CONCLUSION

Kinetic roughening transition was observed around 85 °C in the crystallization of *it*-PB1 tetragonal phase from the melt; a flat growth face, facet, required for regime II growth does not exist below 85 °C. On the contrary, regime II-III transition is not observed in the temperature range of 50 to 110 °C; $\{\ln G + U/R(T - T_V)\}$ presents a single linear dependence on $1/T\Delta T$ described by eq 2 both for faceted and rounded crystals. This is the same paradox pointed out in the growth of *it*-PS in solutions and from the melt. We introduced a step propagation barrier which is proportional to l by considering the 'segmentalized-aligned' activated state in the step propagation processes. Considering this barrier, we can plausibly explain that the regime II-III transition is almost invisible for the crystal growth of *it*-PB1 tetragonal phase.

Acknowledgment. The author MY expresses his sincere thanks Professor Toda (Hiroshima University), Professor Miyaji (Kyoto University) and Professor Fukao (Ritsumeikan University) for valuable discussions and encouragement.

Received: November 15, 2007
Accepted: July 6, 2008
Published: August 22, 2008

REFERENCES

1. J. D. Hoffman and R. L. Miller, *Polymer*, **38**, 315 (1997).
2. J. D. Hoffman, G. T. Davis, and J. I. Lauritzen Jr., in "Treatise on Solid State Chemistry," N. B. Hannay, Ed., Plenum, New York, 1976, Chap. 7, p 497.
3. J. J. Point and J. J. Janimak, *Polymer*, **39**, 7123 (1998).
4. J. P. Armisted and J. D. Hoffman, *Macromolecules*, **35**, 3895 (2002).
5. J. D. Hoffman, *Polymer*, **24**, 3 (1983).
6. M. L. D. Lorenzo, *Polymer*, **42**, 9441 (2001).
7. Y. Miyamoto, Y. Tanzawa, H. Miyaji, and H. Kiho, *J. Phys. Soc. Jpn.*, **58**, 1879 (1989).
8. Y. Tanzawa, *Polymer*, **33**, 2659 (1992).
9. M. Yamashita, Hideki Miyaji, Akitaka Hoshino, and K. Izumi, *Polym. J.*, **36**, 226 (2004).
10. M. Yamashita, A. Hoshino, and M. Kato, *J. Polym. Sci., Polym. Phys. Ed.*, **45**, 684 (2007).
11. M. Yamashita and M. Kato, *J. Appl. Crystallogr.*, **40**, s650 (2007).
12. M. Yamashita and S. Ueno, *Cryst. Res. Technol.*, **42**, 1222 (2007).
13. M. Yamashita and T. Takahashi, *Kobunshi Ronbunshu*, **65**, 218 (2008).
14. M. Yamashita, *J. Cryst. Growth*, **310**, 1739 (2008).
15. H. Miyaji, Y. Miyamoto, K. Taguchi, A. Hoshino, M. Yamashita, O. Sawanobori, and A. Toda, *J. Macromol. Sci.*, **B42**, 867 (2003).
16. M. Yamashita and T. Takahashi, in "Modern Research and Educational Topics in Microscopy," A. Méndez-Vilas, Ed., Formatex Research Center, Badajoz, Spain, 2007, Vol. 2, p 713.
17. A. Turner-Jones, *J. Polym. Sci., Part B: Polym. Lett.*, **1**, 455 (1963).
18. G. Natta, P. Corradini, and I. W. Bassi, *Nuovo Cimento Suppl.*, **15**, 52 (1960).
19. M. Yamashita and M. Kato, *J. Appl. Crystallogr.*, **40**, s558 (2007).
20. Q. Fu, B. Heck, G. Strobl, and Y. Thomann, *Macromolecules*, **34**, 2502 (2001).
21. R. D. Icenogle, *J. Polym. Sci., Polym. Phys. Ed.*, **23**, 1369 (1985).
22. K. Taguchi, H. Miyaji, K. Izumi, A. Hoshino, Y. Miyamoto, and R. Kokawa, *Polymer*, **42**, 7443 (2001).
23. D. M. Sadler, *Polymer*, **24**, 1401 (1983).
24. A. Toda, *J. Chem. Phys.*, **118**, 8446 (2003).

